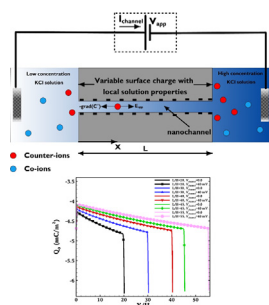


Reverse electrodialysis through nanochannels with inhomogeneously charged surfaces and overlapped electric double layers

Amer Alizadeh, Moran Wang*

Department of Engineering Mechanics and CNMM, Tsinghua University, Beijing, China

GRAPHICAL ABSTRACT



ARTICLE INFO

Article history:

Received 2 April 2018

Revised 28 May 2018

Accepted 30 May 2018

Available online 2 June 2018

Keywords:

Chemically non-isolated interface

Electrokinetic transport

Overlapped electric double layer

Reverse electrodialysis

Representative bulk layer model

Local surface charge

ABSTRACT

Modeling of electro-chemo-mechanical transport phenomena in simple (nanochannel) or complex (nanoporous media) geometries with inhomogeneous surface charge and overlapped electric double layers remains challenging. This bottleneck originates from lack of a comprehensive model to predict the local surface charge density based on the variable local solution properties. This work aims to propose a model, so-called representative bulk layer (RBL), which makes the chemically non-isolated solid-liquid interfaces (due to the electric double layers interaction) as isolated interfaces by introducing a local effective bulk ion concentration. Using RBL together with the electrical triple layer model to provide boundary conditions for the multi-physio-chemical transport equations (PNP + NS), we investigate the reverse electrodialysis (RED) in nanochannels. Our modeling results indicate that the length of an ion-selective membrane not only influences the ionic current but also the logarithm of the slope of current-voltage curve increases linearly with the ratio of nanochannel length to height. This interesting finding inspires us to propose a dimensionless relation for the current-voltage curve that is independent of the nanochannel dimensions. The present contribution numerical framework could shed light on the electro-chemo-mechanical transport mechanism through nanofluidic devices and membranes.

© 2018 Elsevier Inc. All rights reserved.

1. Introduction

For several decades, the electrokinetic transport of ions in simple (micro/nanochannels) or complex (porous media) geometries have been drawn considerable attention due to their extensive

* Corresponding author.

E-mail address: mrwang@tsinghua.edu.cn (M. Wang).

applications from biology, chemical engineering, and environment to geology, petroleum industry, and energy conversion [1–14]. For instance, in the last few years, the electro-chemo-mechanical transport through nanofluidic channels or porous media have been found novel applications in biology [15–20], membrane technology [21,22], energy, environmental, and geophysical engineering [11,23–28]. Despite all the aforementioned applications, the mechanism underlying of electrokinetic transport has remained lag

behind. This lack of understanding is mainly due to ignorance of three coupled factors: (1) electric double layers (EDLs) interaction, (2) local solution properties, and (3) structure of the domain. Although the electro-chemo-mechanical transports in nanochannels [12,13,26] or nanoporous media [1,3,4,7,10,29,30] have been studied theoretically [29#351], however, these studies suffer from limiting to very thin electric double layers (EDL) [31] or constant surface charge density as a fitting parameter. Consequently, omitting the EDLs interaction, local solution properties, and structure effects on the surface charge density for the pores with comparable size to EDL thickness may cause incorrect predictions of the electrokinetic transport mechanism [32]. EDLs interaction eventuates several physical or chemical phenomena, which are of great importance in various applications. Stein et al. [33] and Karnik et al. [34] revealed that the electrical conductance of nano-fluidic channels saturated at a value of the dilute electrolyte which departed significantly from bulk behavior. Pu et al. [27], for the first time, revealed the ion-enrichment and ion-depletion effects (Ion Concentration Polarization (ICP)) when a voltage was applied across a nanochannel. Experiments by Van der Heyden *and co-workers* [35] showed that the streaming current is approximately constant at a dilute aqueous solution but decreases linearly for high-salt concentrations. Kim et al. [26] measured the ionic current generated due to the concentration gradient through a nanochannel as an ion-selective membrane. In order to investigate the effects of EDL interaction, it is crucial to realize the structure of EDL. It is well-realized that when a mineral surface has an interface with an aqueous solution, the surface may be positively or negatively charged [36]. Basically, when an electrolyte, even pure water sometimes, contacts with the chemically reactive solid surface, the solid-liquid interface will be charged because of the physical adsorption and chemical reactions of the ions with the solid-liquid interface [37]. This charge strongly depends on the local properties, such as pH, solution temperature, and ion concentrations [38]. To obtain the surface charge density based on the solution properties, the Basic-Stern (BS) model is the most popular and easy-use one, proposed by Behrens and Grier [39] to bridge the solution properties to surface charge by two simple equations [40]. However, this model considers only the silica dissociation with water and ignores the contribution of salt ions in surface chemical reactions. As a result, it is suitable for dilute solutions [36]. In order to consider the salt-ion contribution to the surface charge, an electrical triple layer (ETL) model was proposed by Davis et al. [41] and developed by Kitamura et al. [37]. The ETL model, generally for the simplest case, has thirteen coupled equations. Despite much more complexity, it may provide accurate and robust predictions of surface charge density and zeta potentials for a much wider range of pH and ionic concentration. However, since the ETL and BS models were proposed based on the absence of any EDL interaction (chemically isolated solid-liquid interfaces), they would not be able to deal with mentioned bottlenecks for nanoscale channels or pores.

By defining a local effective bulk concentration in such simple geometry as straight nanochannel, a few attempts have been accomplished in order to cover the charge regulation of aqueous solution at the solid-liquid interfaces. Huang and Yang [40] proposed a numerical framework in which the electrical surface charge could be determined based on BS model. They introduced two enrichment coefficients for the co- and counter-ions. They defined the effective bulk concentration equal to the ratio of the average of the positive and negative ions in nanochannel cross-section to the reservoir ion concentrations. Wang et al. [42] presented a different enrichment coefficient which is based on the concentration at the middle of the channel. They solved BS model for zeta potential as the electrical boundary conditions. Following the enrichment coefficient, recently, Alizadeh et al. [43] proposed a modified electrical triple layer model to figure out the local

surface charge and zeta potential in a straight nanofluidic channel. By the aid of this model, they demonstrated that how the electrokinetic conductance of nanofluidic channels could be manipulated by varying the inlet solution pH.

In spite of all previous efforts, to the best of the authors' knowledge, there is no theoretical model yet to consider three aforementioned coupled factors (EDLs interaction, local solution properties, and structure of the domain) to obtain the local surface charge in nanochannels or nanopores. In this work, we propose a comprehensive method to, first, make the chemically non-isolated solid-liquid interfaces as isolated interface and then figure out the local effective bulk ion concentration in simple (nanochannel) or complex (porous media) domains. In contrast to the main defect of the previous models [40,42] which made them unsuitable for complex geometries, the main advantage of the present contribution model is that the effective bulk ion concentration is determined based on the aqueous solution properties of a layer in the vicinity of the solid-liquid interface. This method could be employed to the BS or ETL models to predict the local surface charge and zeta potential on the solid-liquid interface. In order to demonstrate the robustness of the proposed method, the electro-chemo-mechanical transports are modeled for streaming potential through two different height nanochannels. Moreover, we investigate the reverse electro dialysis phenomenon by solving the coupled Poisson-Nernst-Planck, and Navier-Stokes equations.

2. Problem definition

The reverse electro dialysis (RED) as a phenomenon with the key role of local surface charge effects has not been fully investigated theoretically yet. Fig. 1 depicts a 2D depiction of a charged nanochannel, which is connected to two reservoirs with different KCl solution concentration based on the fabricated nanochannels-reservoirs platform by Kim *and co-workers* [26]. Ten silica nanochannels in parallel with heights (H) 4, 26, and 80 (nm) were fabricated on a silicon wafer. These nanochannels are 140 (μm) long (L) and 25 (μm) wide (W). In order to measure the current (I_{channel}) passing through the nanochannel, an external electric potential (V_{app}) applied to the electrodes, which generates an external electric field. Owing to the voltage drops at the electrode-solution interface for the different electrolyte solution, thus, the electric potential difference between two ends of the nanochannel (V_{channel}) is obtained as [26]

$$V_{\text{channel}} = V_{\text{app}} - E_{\text{redox}}, \quad (1)$$

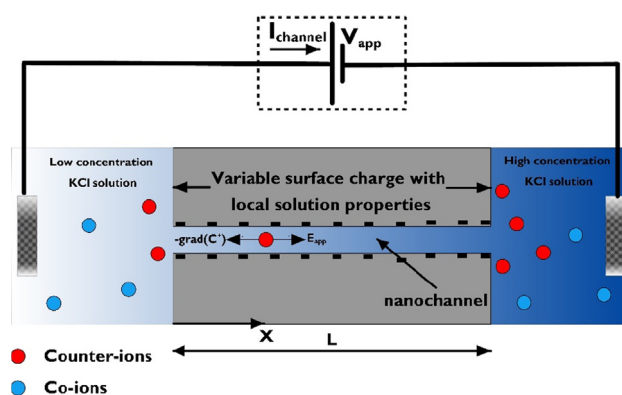


Fig. 1. 2D schematic illustration of the reverse electro dialysis (RED) energy conversion device. The nanochannel has $H = 26$ (nm) and five different lengths which $L/H = 20, 30, 40, 45,$ and 55 subjected to the ion concentration gradient with $C_{\text{Left}} = C_L = 0.1$ (mM) and $C_{\text{Right}} = C_R = 1.0$ (mM). The applied potential (V_{app}) changes from 57.88 (mV) to 97.88 (mV).

where E_{redox} denotes the potential drops at the electrode-solution interface and defined as [44]

$$E_{\text{redox}} = \frac{k_B T}{Ze} \ln \frac{\gamma_{C_H} C_H}{\gamma_{C_L} C_L}, \quad (2)$$

where γ_{C_H} , C_H , γ_{C_L} , and C_L denote the mean activity coefficient of ions at higher KCl solution reservoir, the concentration of ions at higher KCl solution reservoir, mean activity coefficient of ions at lower KCl solution reservoir, and concentration of ions at lower KCl solution reservoir, respectively. In this contribution, according to the experimental results [26], we select the height of the nanochannel equal to $H = 26$ (nm), the lower and higher bulk ion concentration as $C_L = 0.1$ (mM) and $C_H = 1.0$ (mM), respectively, with $\text{pH} = 5.6$. The mean activity coefficient of ions based on the KCl solution concentration would be $\gamma_{C_H} = 0.9648$ and $\gamma_{C_L} = 0.9764$ [45]. As a result, E_{redox} is 0.05788 (V) (Eq. (2)).

An analogy between the generated fluid flow by pressure gradient and ionic current through the nanochannel by concentration gradient indicates that the length of the channel plays a key role in ionic current generated by reverse electrodialysis phenomenon [46]. As mentioned above, the length of the fabricated nanochannels ($L = 140 \mu\text{m}$) would be 5384.6 times greater than the height of the nanochannels ($H = 26$ nm, $L/H = 5384.6$). Consequently, that would cost a huge number of nodes and, as a result, immense time-consuming numerical solution. To deal with this challenge, we investigate the RED phenomenon in nanochannels with $L/H = 20, 30, 40, 45,$ and 55 . For all nanochannel scenarios, it is assumed that the external electric field would be the same as the experimental setup ($E_{\text{app}} = V_{\text{app}}/L$). Later, we will demonstrate that based on the modeling results for these five nanochannel cases, one can predict the nanochannel ionic current with $L/H = 5384.6$. The physical properties of the solution are the same as those mentioned in Table 1.

2.1. Mathematical models and numerical methods

The electrokinetic transport phenomena of multi-species ions are governed by the Nernst-Planck equations coupled with the Poisson and Navier-Stokes equations, which leads to full consideration of the electro-chemo-mechanical transport phenomena. For hydrodynamic transport, the Navier-Stokes equations are [47]

$$\begin{aligned} (a) \quad \frac{\partial \rho}{\partial t} + \nabla \cdot (\rho \mathbf{u}) &= 0, \\ (b) \quad \frac{\partial (\rho \mathbf{u})}{\partial t} + \mathbf{u} \cdot \nabla (\rho \mathbf{u}) &= -\nabla p + \nabla \cdot [\nu \nabla (\rho \mathbf{u})] - \rho_e (\nabla \phi + \nabla \Psi), \end{aligned} \quad (3)$$

where ρ (kg m^{-3}) is the density of the electrolyte, \mathbf{u} (m/s) is the flow velocity vector, t (s) is time, p (Pa) is the fluid pressure, ν (m^2/s) is the momentum diffusivity, $\nabla \phi$ is the external electric potential field, $E_x = -\nabla \phi_x$, $\nabla \phi_y = 0$, and $\nabla \Psi$ represent the internal electric potential field, which is obtained by solving the Poisson equation

for free net charge density ρ_e (m^{-3}). Regarding the governing equation for ion transport, the mass conservation equation for i th ion species in an electrolyte is [48,49]

$$\frac{\partial C_i}{\partial t} + \nabla \cdot \left(-D_i \left(\frac{eZ_i}{k_B T} C_i \nabla \Psi + \nabla C_i \right) + C_i \mathbf{u} \right) = 0, \quad (4)$$

in which the flux of the ions $\mathbf{J}_i = -D_i \left(\frac{eZ_i}{k_B T} C_i \nabla \Psi + \nabla C_i \right) + C_i \mathbf{u}$ and the ionic current is obtained as $I_{\text{channel}} = \sum_{i=1}^N Z_i e \mathbf{J}_i$. In Eq. (4), C_i (m^{-3}) denotes the number density of the i th ion, D_i (m^2/s) the ionic diffusivity, Z_i the i th valence, and e (C) the elementary charge. The local internal electric potential field, Ψ , which is caused by the ion distribution, is governed by the Poisson equation as

$$\nabla^2 \Psi = -\frac{\rho_e}{\epsilon_r \epsilon_0}, \quad (5)$$

where ρ_e is defined as $\sum_i e Z_i C_i$. To solve the Poisson equation, we need to obtain the zeta potential of the solid-liquid interfaces locally. For this purpose, the ETL model is nominated to predict the zeta potential. However, the conventional ETL model was developed based on the isolated solid-liquid interface [36] which makes it unsuitable for such confined domains like nanochannels or nanopores. According to the ETL model, the isolated silica surfaces acquire electric charge due to the typical chemical reactions of the surface as [37]



where K_{a1}^{int} , K_{a2}^{int} , and K_M^{int} represent the associated equilibrium constants for chemical reactions, respectively. Three layers in this model demonstrate the inner- and outer-Helmholtz planes and the start edge of the diffuse layer. In the pH range of 3–9, based on the law of mass action and considering an effective bulk concentration (should be determined later), the set of ETL equations could be found in details elsewhere [36,37]. However, in order to introduce the RBL to ETL model, we re-define four equations of the ETL set of equations as

$$K_{a1}^{\text{int}} = \frac{\sigma_{\text{SiOH}}}{\sigma_{\text{SiOH}_2^+}} C_{\text{H}^+,b}^{\text{eff}} \exp \left(-\frac{e\Psi_0}{k_B T} \right), \quad (9)$$

$$K_{a2}^{\text{int}} = \frac{\sigma_{\text{SiO}^-}}{\sigma_{\text{SiOH}}} C_{\text{H}^+,b}^{\text{eff}} \exp \left(-\frac{e\Psi_0}{k_B T} \right), \quad (10)$$

$$K_M^{\text{int}} = \frac{\sigma_{\text{SiOM}}}{\sigma_{\text{SiO}^-}} \left(\frac{1}{C_{\text{M}^+,b}^{\text{eff}}} \right) \exp \left(\frac{e\Psi_\beta}{k_B T} \right), \quad (11)$$

$$Q_d = -\sqrt{8\epsilon_r \epsilon_0 k_B T n_{s,b}^{\text{eff}}} \sinh \left(\frac{e\Psi_d}{2k_B T} \right), \quad (12)$$

where $n_{s,b}^{\text{eff}} = 1000 N_A (C_{\text{M}^+,b}^{\text{eff}} + C_{\text{H}^+,b}^{\text{eff}})$. Q_d represents the surface charge on the d-plane (the start edge of the diffuse layer). $C_{\text{H}^+,b}^{\text{eff}}$ and $C_{\text{M}^+,b}^{\text{eff}}$ denote the effective bulk ion concentration for H^+ and M^+ which have to obtain locally for nanochannel with the overlapped electric double layer.

2.1.1. Representative bulk layer (RBL) model

In this section, we propose a comprehensive model to make the non-isolated solid-liquid interface as isolated interface by introducing an effective bulk ion concentration. From a physical point of view, a chemically reactive surface interacts with the aqueous

Table 1
Constants parameters for KCl aqueous solution at $T = 298$ (K).

Value [Unit]	Variable
$5.6 \times 10^{-6} \sim 1.0$ (M)	n_b
78.54	ϵ_r
8.854×10^{-12} (C/V × m)	ϵ_0
999 (kg/m ³)	ρ
1×10^{-3} (Pa s)	μ
19.57×10^{-10} (m ² /s)	D_{K^+}
20.3×10^{-10} (m ² /s)	D_{Cl^-}

solution near to the solid-liquid interface, which causes the surface charge on the solid surface. This charge is strongly dependent on the solution local acidity (pH), temperature, and contribution of the counter-ions to the chemical reactions with the surface [36]. To predict the surface charge, the ETL or BS model could be employed in which the local acidity and counter-ions concentration near to the solid-liquid interface have been correlated with the reservoir bulk concentration through the Boltzmann ion distribution [37]. However, for such a confined space like nanochannels or nanopores with low ionic strength, the EDLs are strongly interact and as a result, the reservoir bulk concentration would not be available anymore in the bulk space of the channel or pore. Accordingly, it seems to be crucial to define an effective bulk concentration in which the effects of three-coupled factors (EDLs interaction, local solution properties, and structure of the domain) have been comprised. Moreover, any proposed approach which aims to tackle the remained bottleneck of predicting the local surface charge in simple and complex geometries requires to (1) consider EDL interactions when they are overlapped; (2) recover the reservoir bulk concentration when there is no EDL overlap [33]. To this aim, we propose a model with which the local effective bulk concentration could be obtained based on the electrochemical data extracted from a region near to the solid-liquid interface. Fig. 2 illustrates our strategy for an unstructured domain. It is demonstrated that this region near to the interface could be a thin layer with arbitrary thickness ($\delta = r_b$) which we so-called *representative layer*. Obviously, this layer is composed of the background aqueous solution with hydroxyl, hydronium, co-, and counter-ions. The concentration of these ions depends on several factors such as the local surface charge, pore size, and solid material.

In order to describe the proposed idea in details, first, we consider a complex geometry (Fig. 3a) as a nanopore. Second, we select a representative layer (thin layer with thickness $\delta = r_b$) close enough to the solid-liquid interface (Fig. 3b). Physically, the representative layer possesses the characteristic properties of the background aqueous solution properties and the charge regulation effects due to the strong interaction of the EDLs in nanochannel or nanopore. As the next step, we separate all the representative layers from the rest of the pore domains (Fig. 3c). In order to make a chemically isolated solid-liquid interface based on the electrochemical data of the separated representative layer, we add an isolator aqueous solution layer to the representative layer (Fig. 3d). We note that the isolator layer must have the same physical prop-

erties (i.e., viscosity, density, temperature etc.) in accordance with the reservoir aqueous solution. In order to make sure that the solid-liquid interface will be treated as an isolated interface, we choose the isolator layer thickness (Fig. 3d); h , large enough that at $y = h$ the electric potential reaches to $\Psi = 0$. Consequently, one can indicate that for a solid-liquid interface, when $y \rightarrow h$, the electric potential $\Psi \rightarrow 0$. This eventuates to the fact that the concentration of the ions at $y = h$ is equal to a bulk concentration which is so-called the effective bulk ion concentration ($n_0 = C_{\text{eff}}$, Fig. 3d). We have to note that the effective bulk concentration may not be equal to the reservoir bulk ion concentration due to the local solution properties, EDLs interaction, and the pore domain structure. As a result, there is a new aqueous solution which: (1) is in contact with an isolated solid-liquid interface; (2) has an effective bulk concentration; (3) the concentration of the ions and electrical potential near to the walls have been originated from the pore domain under consideration. Since the proposed model eventuates to an effective bulk ion concentration from the representative layer near to the solid-liquid interface, we name it as representative bulk layer (RBL) model. Later, in this section, we will show that the RBL model does not only able to predict the rigorous effective bulk concentration for overlapped EDLs but also it could return the reservoir bulk concentration as the effective bulk concentration for the non-overlapped EDLs regime.

In order to obtain the effective bulk ion concentration, we consider the Nernst-Planck equation for the representative bulk layer. While this layer is selected close enough to the solid-liquid interface and for an isothermal solution, the steady-state Nernst-Planck equation in the y -direction results as [47]

$$D_i \frac{\partial^2 C_i}{\partial y^2} + \frac{eZ_i D_i}{k_B T} \frac{\partial^2 \Psi}{\partial y^2} = 0.0, \quad (13)$$

where $u_y \cong 0.0$. Integrating both sides of Eq. (13) in the y -direction from 0 to r_b , the ion distribution near to the interface is obtained

$$C_i(y) = C_i^{r_b} \exp\left(-\frac{eZ_i}{k_B T} (\Psi(y) - \Psi^{r_b})\right), \quad 0 \leq y \leq r_b, \quad (14)$$

where $C_i^{r_b}$ and Ψ^{r_b} denote the concentration of i th ion and internal electric potential at $y = r_b$, respectively.

Considering the fact that the balance of diffusion and electromigration governs the ion distribution in the representative layer, one can indicate that the new electrolyte solution (the

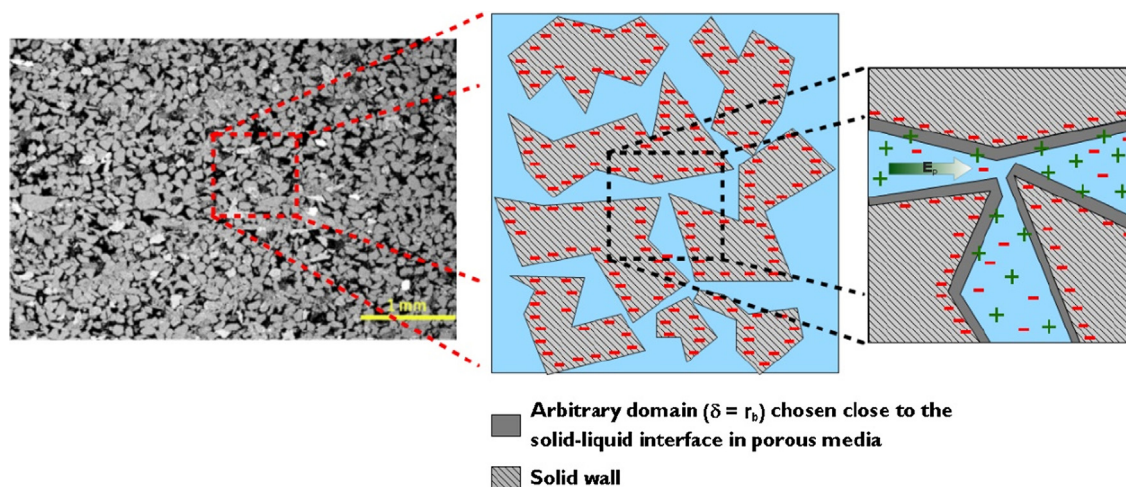


Fig. 2. A general illustration of the arbitrary thin layer near to the solid-liquid interface of a granular porous media. The patterned unstructured shapes demonstrate the solid grains with negative surface charge. The selected layers near to the solid surfaces are depicted by thin gray un-patterned layers. The proposed approach could be employed for a simple straight channel to a complex domain like porous media.

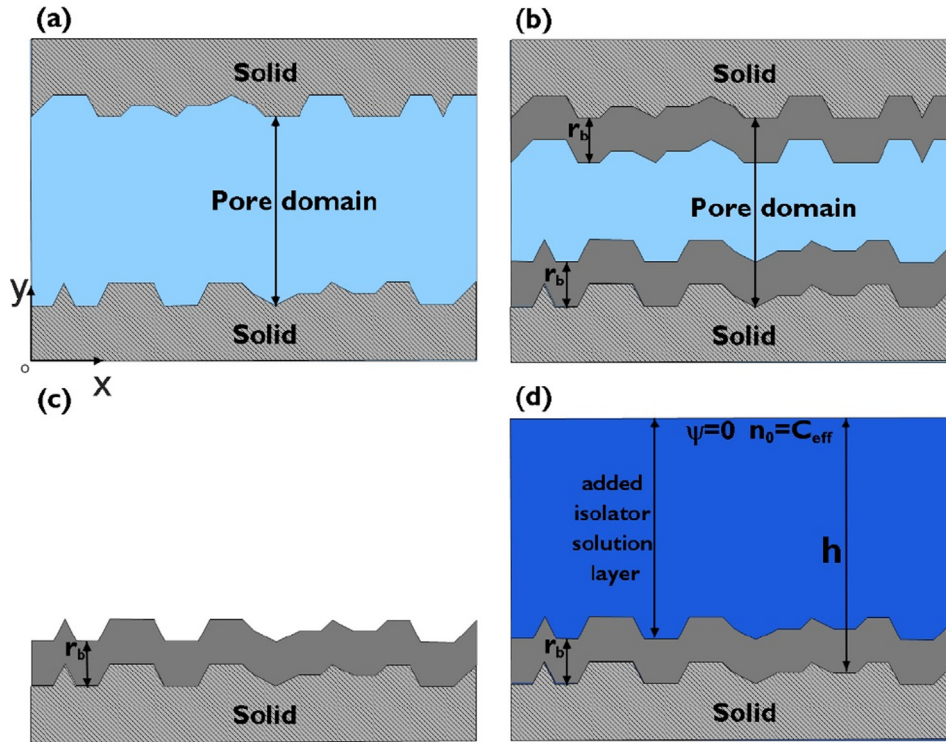


Fig. 3. Schematic illustration of the representative-bulk layer (RBL) model to find out the local effective bulk concentration. (a) The pore domain with complex geometry. (b) Specifying the representative layer close enough to the solid-liquid interface. (c) Separating the selected representative layer near to the solid-liquid interface from the remained solution. (d) Adding the isolator aqueous solution layer to the selected representative layer near to the solid wall.

representative layer and the added isolator solution layer) has not ionic convection in the y -direction. On the other hand, the new solution, in fact, has an effective bulk ion concentration, $C_{\text{eff}} = C_{i,b}^{\text{rb}}$, at $y = h$. Consequently, under these conditions, the Boltzmann distribution is valid and governs the ion distribution in the y -direction as

$$C_i(y) = C_{i,b}^{\text{rb}} \exp\left(-\frac{eZ_i}{k_B T} \Psi(y)\right), \quad 0 \leq y < h, \quad (15)$$

If we equate Eqs. (14) and (15) for the representative layer region ($0 \leq y \leq r_b$), the related local effective bulk concentration $C_{i,b}^{\text{rb}}$ obtains

$$C_{i,b}^{\text{rb}} = \frac{C_i^{\text{rb}}}{\exp\left(-\frac{eZ_i}{k_B T} \Psi^{\text{rb}}\right)}, \quad (16)$$

where C_i^{rb} denotes the predicted effective bulk ion concentration for when the representative layer is selected with a thickness $\delta = r_b$.

Considering the overlapped and non-overlapped EDLs regime, recently, Zhang and Wang [31] classified the electroosmotic flow regimes by inspiring the Knudsen number. They defined $M = 1/\kappa H$ and found that for $0.1 \leq M \leq 1$ the EDLs are partially overlapped and for when $M > 1$, the EDLs would be fully overlapped. Inspiring Eq. (16) and what mentioned for overlapped and non-overlapped EDLs regime, our numerical experiences showed that for the partially or fully overlapped EDLs ($\kappa H \leq 6$ or $M \geq 1/6$), it would be more reasonable to employ the mean ionic concentration, $\frac{1}{r_b} \int_0^{r_b} C_i(y) dy$, for range $0 \leq y \leq r_b$, instead of C_i^{rb} . In addition, because for the fully overlapped EDLs scenario, the internal electric potential does not change significantly inside of the EDL, therefore we define a constant reference electric potential, Ψ_{ref} , instead of Ψ^{rb} . On the other hand, for the non-overlapped EDLs regime ($\kappa H > 6$ or $M < 1/6$), Eq. (16) predicts the reservoir bulk ion concentration (n_b). Eventually, based on what mentioned

above, we propose the local effective bulk concentration for a distance r_b from the wall as

$$C_{i,b}^{\text{rb}} = \begin{cases} \frac{\frac{1}{r_b} \int_0^{r_b} C_i(y) dy}{\exp\left(-\frac{eZ_i}{k_B T} \Psi^{\text{ref}}\right)} \left(\frac{H}{\lambda} = \frac{1}{M}\right) \leq 6 \\ \frac{C_i^{\text{rb}}}{\exp\left(-\frac{eZ_i}{k_B T} \Psi^{\text{rb}}\right)} \left(\frac{H}{\lambda} = \frac{1}{M}\right) > 6 \end{cases}, \quad (17)$$

where H is the specific height of the channel or the average pore size of the porous media, λ is the Debye screening length for EDL thickness which is defined for a monovalent electrolyte solution as $\lambda^{-1} = \sqrt{\frac{2e^2 n_b}{\epsilon_r \epsilon_0 k_B T}}$. We have to note that in Eq. (17), it is assumed that the EDLs interact even when H is six times greater than the Debye screening length. The main reason in favor of this consideration is that, realistically, the thickness of the EDL is greater than the Debye length [31,50]. Consequently, we assume that when the thickness of the EDLs is three times smaller than the Debye length, there would be non-overlapped EDLs regime.

In Eq. (17), for aqueous solutions with $H/\lambda \leq 6$ or $M \geq 1/6$, we define the reference electric potential as:

$$\Psi_{\text{ref}} = \frac{\int_{1.0 \times 10^{-6}}^{n_b^m} \zeta(n_b) dn_b}{n_b^m - 1.0 \times 10^{-6}}, \quad (18)$$

where n_b is the reservoir bulk concentration changes from 1.0×10^{-6} (M) to n_b^m (M). The n_b^m is the maximum reservoir bulk concentration which for a specified H , the $H/\lambda = 6$ or $M = 1/6$. $\zeta(n_b)$ is the zeta potential as a function of reservoir bulk ion concentration which is predicted by the ETL or BS model and assumed to be obtained for an isolated silica surface placed in an infinite aqueous solution [36].

It is important to note that Eq. (17) demonstrates how the RBL model could predict the local effective bulk concentration based on

the electrochemical data near to the solid-liquid interfaces. Moreover, the definition of the local effective bulk concentration (Eq. (17) is based on the numerical results that are updating in each iteration. Consequently, this definition comprises all the effects of complex geometries, local solution properties, EDL interaction on the local effective bulk concentration without any extra efforts. Recalling the ETL set of equations (Eqs. (9–12), presently, we are able to define the effective bulk ion concentration as

$$C_{H^+,b}^{eff} = \begin{cases} \frac{\frac{1}{r_b} \int_0^{r_b} C_{H^+}(y) dy}{\exp\left(\left(\frac{-eZ_i}{k_B T}\right) \Psi^{ref}\right)} \left(\frac{H}{\lambda} = \frac{1}{M}\right) \leq 6 \\ \frac{C_{H^+}^{rb}}{\exp\left(\left(\frac{-eZ_i}{k_B T}\right) \Psi^{rb}\right)} \left(\frac{H}{\lambda} = \frac{1}{M}\right) > 6 \end{cases},$$

$$C_{M^+,b}^{eff} = \begin{cases} \frac{\frac{1}{r_b} \int_0^{r_b} C_{M^+}(y) dy}{\exp\left(\left(\frac{eZ_i}{k_B T}\right) \Psi^{ref}\right)} \left(\frac{H}{\lambda} = \frac{1}{M}\right) \leq 6 \\ \frac{C_{M^+}^{rb}}{\exp\left(\left(\frac{eZ_i}{k_B T}\right) \Psi^{rb}\right)} \left(\frac{H}{\lambda} = \frac{1}{M}\right) > 6 \end{cases}, \quad (19)$$

and eventually, closing the set of ETL equations. In Eq. (19), Ψ^{ref} is obtained by Eq. (18). It is worth mentioning that the constant input parameters for the ETL model are the same as those mentioned in Wang et al. [36].

To solve the governing equations, we employed the coupled lattice Boltzmann methods which are solving in an iteration procedure and discussed in details elsewhere [47]. The RBL associated with the ETL model has predicted the local electrical boundary condition for each node of the solid-liquid interface in an iterative procedure coupled with PNP + NS.

2.1.2. Electrochemical Donnan equilibrium boundary conditions

It should be noted that in this contribution, in order to reduce the time costs for modeling RED, we ignored the presence of the inlet and outlet reservoirs in our models. However, the effects of the reservoirs on the concentrations of the co-ions, counter-ions, and the electric potential at the inlet and outlet of the nanochannel could be considered by employing the Donnan equilibrium theory [51] as

$$(a) C_{i,l} = \sqrt{\left(\frac{\sigma_{r,l}}{Z_i e N_A H}\right)^2 + (C_{r,l})^2} - \frac{\sigma_{r,l}}{Z_i e N_A H},$$

$$(b) C_{i,o} = \sqrt{\left(\frac{\sigma_{r,r}}{Z_i e N_A H}\right)^2 + (C_{r,r})^2} - \frac{\sigma_{r,r}}{Z_i e N_A H}, \quad (20)$$

where $C_{i,l}$ and $C_{i,o}$ denote the concentration of the i th ion (in mol/m³) at the inlet and outlet of the nanochannel, respectively. In addition, $C_{r,l}$ and $C_{r,r}$ represent the left and right reservoirs KCl concentration (in mol/m³), respectively. $\sigma_{r,l}$ and $\sigma_{r,r}$ denote the left and right reservoirs surface charge density (in C/m²), respectively, which are obtained by employing the RBL associated with the ETL model. Considering the electric potential (Ψ) at both ends of the nanochannel [51]

$$(a) \Psi_l = \Psi_L + \frac{k_B T}{Ze} \ln \left(\frac{\sqrt{\left(\frac{\sigma_{r,l}}{e N_A H}\right)^2 + (C_{r,l})^2} + \frac{\sigma_{r,l}}{e N_A H}}{C_{r,l}} \right),$$

$$(b) \Psi_o = \Psi_R + \frac{k_B T}{Ze} \ln \left(\frac{\sqrt{\left(\frac{\sigma_{r,r}}{e N_A H}\right)^2 + (C_{r,r})^2} + \frac{\sigma_{r,r}}{e N_A H}}{C_{r,r}} \right), \quad (21)$$

where Ψ_l and Ψ_o denote the inlet and outlet electric potential of the nanochannel. Ψ_L and Ψ_R represent the electric potential at the inlet and outlet of the left and right reservoirs, respectively. Considering the fabrication of the RED device [26], there would

not be any surface charge possession on the walls of the reservoir ($\Psi_L = \Psi_R = 0$).

3. Results and discussion

3.1. Validation and benchmarks

We investigate the effect of the representative bulk layer thickness on the streaming potential of a simple nanochannel. Fig. 4 shows a simplified 2D model of a charged silica nanochannel. The dimensions of the nanochannel are chosen as the same as that fabricated by Van der Heyden and co-workers [35] with length $\equiv L = 4.5$ (μm) and width $\equiv W = 50$ (μm). Two heights, $H = 70$ (nm) and 140 (nm) are considered. The inlet of the nanochannel is connected to a pressurized reservoir, while the opposite side is left open to a non-pressurized reservoir at $T = 298$ (K). In order to study the effect of representative layer thickness ($\delta = r_b$) on modeling results, four different H/r_b is prescribed as 125.5, 50.2, 10.04, and 6.25 for both channel heights. The KCL concentration at reservoir varies from 5.6 (μM) to 1 (M). It is assumed that the acidity and the temperature of the solution are constant everywhere in the channel with $\text{pH} = 8$ and $T = 298$ (K), respectively. Table 1 shows the constant parameters in the problem at $T = 298$ (K).

Let us consider a pressure-driven flow through a charged nanochannel in the absence of any external electric field. The motion of the ions by the applied pressure gradient causes an electrical current which is so-called the streaming current (I_{str}) [35]

$$I_{str} = w \int \rho_e(y) u(y) dy, \quad (22)$$

where w denotes the width of the nanochannel. Streaming conductance, S_{str} , is defined as the streaming current per unit applied pressure gradient [35,42,52]

$$S_{str} = \frac{w}{\Delta P} \int \rho_e(y) u(y) dy, \quad (23)$$

It is shown that for a specified silica nanochannel height, for various applied pressure gradients, S_{str} is constant [35]. To investigate the fully considered electro-chemo-mechanical transport phenomena, the governing equations mentioned at Section 2.1 are subjected to the boundary conditions as follows

For Navier-Stokes equations:

$$y = 0 \rightarrow u = v = 0, \quad y = H \rightarrow u = v = 0,$$

$$x = 0 \rightarrow \frac{\partial u}{\partial x} = v = 0, \quad p = P_{inlet} > P_{atm}, \quad (24)$$

$$x = L \rightarrow \frac{\partial u}{\partial x} = \frac{\partial v}{\partial x} = 0, \quad p = P_{atm}.$$

where u and v represent the fluid flow velocity along the x - and y -direction of the nanochannel, respectively. The zero normal flux

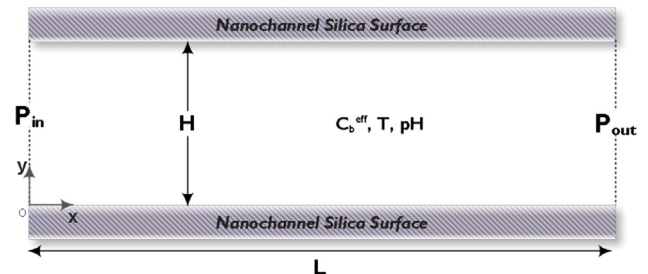


Fig. 4. Schematic of the simplified 2D nanochannel. The pressure boundaries are P_{in} and P_{out} , C_b^{eff} the effective bulk concentration, T the solution temperature, pH the acidity of the solution, H and L the height and length of the nanochannel, respectively.

conditions for the ionic species on the solid-liquid interface, S , is applied as

$$(\mathbf{V} \cdot \mathbf{J}_i)_S = 0, \quad (25)$$

where $\mathbf{V} = u\mathbf{i} + v\mathbf{j}$ represents the velocity of the fluid flow. The inlet of the nanochannel is subjected to the inlet solution ionic species concentrations

$$x = 0 \rightarrow C_i = C_{i,\text{inlet}}, \quad (26)$$

$$x = L \rightarrow \frac{\partial C_i}{\partial x} = 0, \quad (27)$$

The boundary conditions governing the Poisson equation would be defined as [53]

$$\begin{aligned} x = 0, & \rightarrow \Psi = 0, \\ x = L, & \rightarrow \frac{\partial \Psi}{\partial x} = 0, \\ y = 0 \text{ and } y = H & \rightarrow \Psi = \Psi_d, \end{aligned} \quad (28)$$

where Ψ_d , the zeta potential, would be obtained as the output parameter of the ETL model (Section 2.1.).

Fig. 5 shows the streaming conductance of two nanochannel heights versus the reservoir KCl concentrations. It should be noted that r_b for each nanochannel is prescribed in a way that H/r_b would be equal for both of the channel heights. Fig. 5a shows the streaming conductance of channel $H = 70$ (nm) with four different H/r_b . Modeling results show that by increasing the reservoir concentration the streaming conductance is increased while it is being saturated up to a maximum value. However, increasing the reservoir concentration beyond the maximum saturated value will decrease the streaming conductance. Fig. 5a shows a good agreement between the present work predictions and the experimental measurements by Van der Heyden et al. [35]. Considering the effect of r_b , Fig. 5a illustrates that increasing the r_b reduces the accuracy of the predicted streaming conductance compared with experimental results for strong overlapped EDLs interaction.

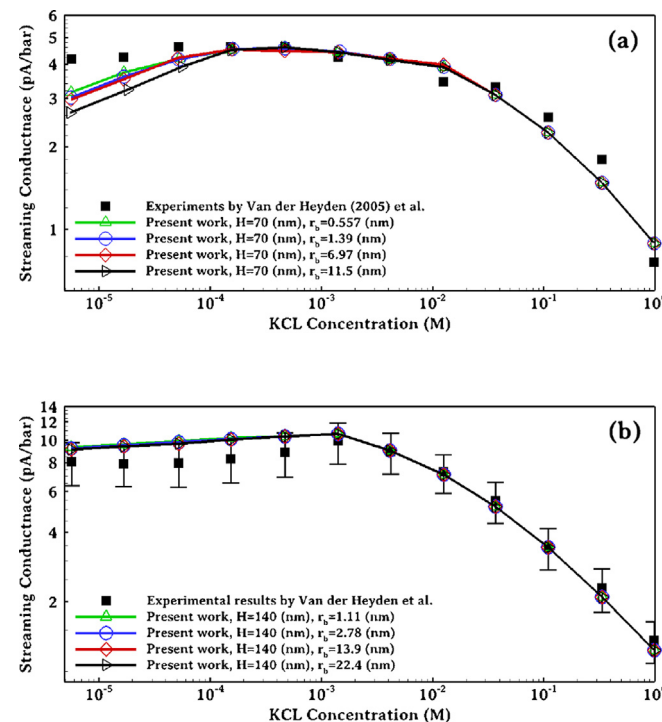


Fig. 5. Streaming conductance versus reservoir KCl concentration for two silica nanochannels (a) $H = 70$ (nm), (b) $H = 140$ (nm) with four different r_b .

Obviously, for higher reservoir concentrations, while the interaction of the EDLs decreases, it is expected that the present study numerical framework predicts same streaming conductance for four H/r_b (Fig. 5a).

Fig. 5b shows the streaming conductance of three different H/r_b for a silica nanochannel with $H = 140$ (nm). Considering the streaming conductance versus reservoir concentration, (Fig. 5b) it is revealed that the nanochannels with $H = 70$ (nm) and $H = 140$ (nm) have similar behavior by increasing the reservoir bulk concentration. However, it should be mentioned that for the nanochannel of Fig. 5b, by increasing the representative layer thickness (r_b), there would not be a significant effect on the predicted streaming conductance. Fig. 5b elucidates the fact that even with increasing the nanochannel height, the proposed numerical framework predictions have good agreement with the experimental data. Comparing the accuracy of the two predicted streaming conductance (Fig. 5a and b), one can indicate that the results for the nanochannel with $H = 140$ (nm) is more accurate. The main reason in favor of this fact is that for higher channel height, the EDLs interaction would be weaker. Consequently, similar to those mentioned for the behavior of higher reservoir concentration, increasing the r_b would not have significant effects on the results.

3.2. Reverse electrodialysis (RED) with inhomogeneous surface charge

In order to show the robustness of the present work numerical framework, in this section, we study the ionic current through an ion-selective nanochannel in reverse electrodialysis. According to the ion selectivity essence of the charged nanochannels or nanomembranes, by imposing a concentration gradient at the inlet and outlet reservoirs, due to the Gibbs free energy of mixing, the diffusion phenomenon forces counter-ions to pass through the nanochannel while the co-ions repel. Since there is non-zero net electric charge density ($\rho_e \neq 0$) within the nanochannel, as a result, an ionic current passes through the ion-selective nanochannel. This ionic current generates electric current. This energy conversion phenomenon is called reverse electrodialysis [26].

By solving the defined problem (Section 2) for five different nanochannels with $L/H = 20, 30, 40, 45,$ and 55 , the I-V curve is obtained by changing the applied electric potential (V_{app}) from 57.88 (mV) to 97.88 (mV) for each nanochannel. We re-emphasize that the strength of the applied electric field is same for all nanochannels ($E_{\text{app}} = V_{\text{app}}/L$). Our modeling results show that the slope of the I-V curve essentially changes as a function of L/H . To compare the slope of I-V curves for our five nanochannel scenarios, we define the slope of I-V curve as

$$\theta = \frac{I_0 - I_V}{I_0 V} = \frac{1 - I_V/I_0}{V}, \quad (29)$$

where I_0 and I_V represent the nanochannel ionic current when $V_{\text{channel}} = 0.0$ and V , respectively. Fig. 6a shows the $\log(\theta)$ versus $\log(10^{-1} L/H)$. It is shown that the logarithm of slope presents a roughly linear or second order relation with L/H . By employing the least squares method to fit a first order ($\log(\theta) = -1.0244 + 0.89 \log(10^{-1} L/H)$) and second order ($\log(\theta) = -0.295 (\log(10^{-1} L/H))^2 + 1.85 \log(10^{-1} L/H) - 1.458$) curves to our modeling results (blue symbols), one can extrapolate the $\log(\theta)$ for nanochannel when $L/H = 5384.6$.

To obtain the I-V curve for the fabricated nanochannel with $L/H = 5384.6$, essentially, in addition to the slope of the I-V curve, we need to figure out the nanochannel ionic current when $V_{\text{channel}} = 0.0$. To this aim, we re-utilize the extrapolation strategy. Fig. 6b indicates the $\log(I_{V=0})$ as a function of $\log(10^{-1} L/H)$. Obviously, it is shown that the $\log(I_{V=0})$ demonstrates a linearly decreasing relationship by increasing the $\log(10^{-1} L/H)$. Consequently, by

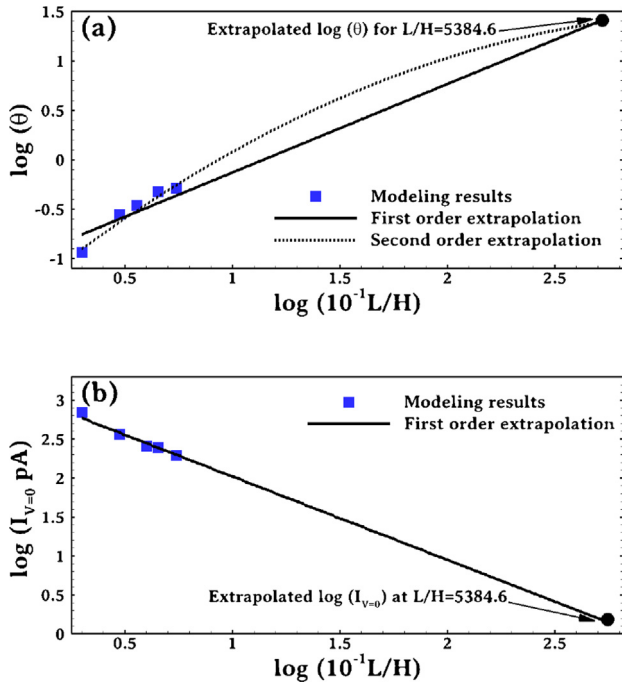


Fig. 6. The extrapolated (a) slope of the I-V curve by first order $\log(\theta) = -1.0244 + 0.89 \log(10^{-1} L/H)$ and second order $\log(\theta) = -0.295 (\log(10^{-1} L/H))^2 + 1.85 \log(10^{-1} L/H) - 1.458$ extrapolation, and (b) ionic current through the nanochannel at $V_{\text{channel}} = 0.0$ by first order $\log(I_{V=0}) = 3.089 - 1.07 \log(10^{-1} L/H)$ extrapolation, for $L/H = 5384.6$.

using the least squares method we fit a first order curve as $\log(\theta) = 3.089 - 1.07 \log(10^{-1} L/H)$. Finally, the $I_{V=0}$ for when $L/H = 5384.6$ is obtained by extrapolation. By employing the obtained slope of the

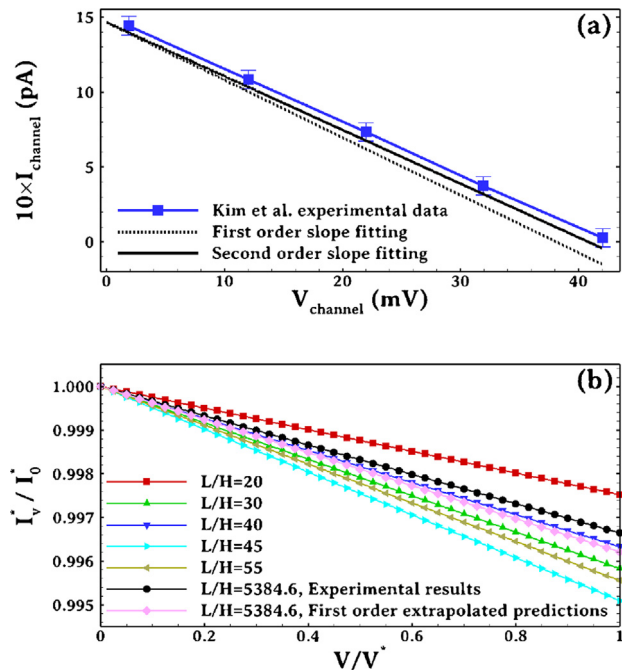


Fig. 7. The (a) prediction of the nanochannel ionic current versus nanochannel potential based on the present work model compared with experimental data [26]. Considering the results of the first order and second order slope fitting have shown more accurate results for second order slope fitting. (b) the dimensionless I-V curves for different L/H scenarios compared with the experiments demonstrate the nanochannel ionic current is roughly independent of L/H.

I-V curve and $I_{V=0}$ for nanochannel with $L/H = 5384.6$, the I-V curve for a nanochannel with $L/H = 5384.6$ could be figure out. Fig. 7a demonstrates good agreement of present work prediction compared with experimental measurements [26] specifically for second order fitting of slope (solid line). However, the predicted I-V curve based on the first order slope fitting (dashed line) also demonstrates an acceptable range of deviations from experiments.

The linear behavior of $\log(\theta)$ and $\log(I_{V=0})$ versus $\log(10^{-1} L/H)$ (Fig. 6) inspiring the fact that there would be a dimensionless definition of I-V curves which could be independent of nanochannel L/H. Recalling the first order relationship of $\log(\theta)$ with $\log(10^{-1} L/H)$

$$\log \theta = -1.024 + 0.895 \log \left(10^{-1} \frac{L}{H} \right), \quad (30)$$

one can rewrite it as

$$\theta^* = \frac{\theta}{\left(10^{-1} \frac{L}{H} \right)^{0.895}} = 10^{-1.024}, \quad (31)$$

which denotes that if θ normalized by $(10^{-1} L/H)^{0.895}$ and defined as $\theta^* = \theta / (10^{-1} L/H)^{0.895}$, then θ^* would be independent of nanochannel L/H variations. Regarding the $I_{V=0}$, the first order relationship with $\log(10^{-1} L/H)$

$$\log(I_{V=0}) = 3.089 - 1.07 \log \left(10^{-1} \frac{L}{H} \right), \quad (32)$$

which can rearrange as

$$I_{V=0}^* = \frac{I_{V=0}}{\left(10^{-1} \frac{L}{H} \right)^{-1.07}} = 10^{3.089}, \quad (33)$$

Similar to what we mentioned for θ^* , we define $I_{V=0}^* = I_{V=0} / (10^{-1} L/H)^{-1.07}$ which represents that the ionic current at $V_{\text{channel}} = 0$ could be normalized via $(10^{-1} L/H)^{-1.07}$. Eventually, the general relation for I-V curve which is independent of L/H could be as

$$\frac{I_V^*}{I_{V=0}^*} = 1.0 - \frac{V}{V_{\text{ref}}} \frac{\theta^*}{I_{V=0}^*}, \quad (34)$$

whereas $I_{V=0}^* = 10^{3.089}$, $\theta^* = 10^{-1.024}$, $I_V^* = I_V / (10^{-1} L/H)^{-1.0705}$ and V_{ref} denotes the reference electric potential which we assume equal to 40 (mV). Fig. 7b demonstrates the dimensionless I-V curves based on Eq. (34) for all nanochannels with five different amounts of L/H,

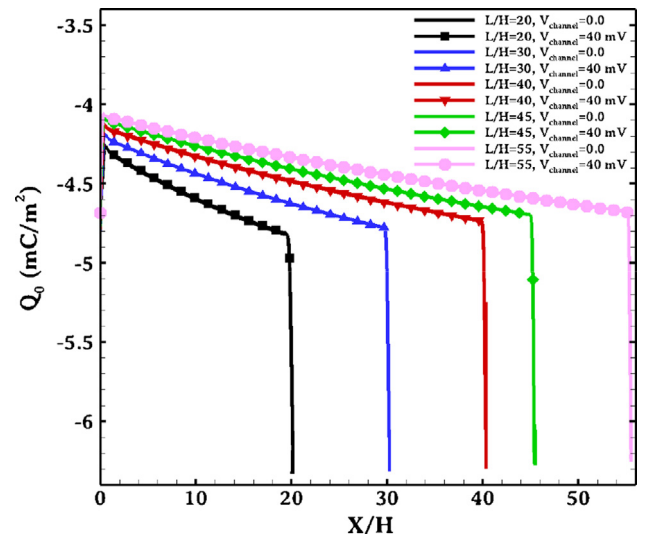


Fig. 8. The surface charge density (Q_0) distribution along the five nanochannels under consideration obtained by the proposed numerical framework.

the predicted results for $L/H = 5384.6$, and the experimental results. As expected, it is shown that the I-V curves for different L/H nanochannels could be approximately identical. Eq. (34) reveals an important fact that by a proper ionic current normalizing, one can figure out an independent I-V curve from the nanochannel L/H.

It is well realized that the ionic current through the nanochannels mainly dominated by the surface charge on the solid-liquid interfaces [54]. In order to have detail insight into the surface charge distribution along the considered nanochannels in RED, Fig. 8 demonstrates the realistic surface charge density that is obtained based on the RBL with ETL model. As we expected, modeling results showed that the surface charge for all nanochannel scenarios would be decreasing along the channel due to the imposed concentration gradient at two reservoirs. In addition, it is demonstrated that by increasing the nanochannel L/H, the absolute amount of the surface charge density would be decreased which supports our findings for ionic current as a function of L/H which discussed in details above.

4. Conclusions

In this contribution, we proposed a numerical framework to predict the local surface charge density by isolating the chemically non-isolated solid-liquid interfaces. The isolation of the interface was conducted based on the solution properties which were extracted from a thin layer (representative layer) near to the interface (representative bulk layer model). By introducing the representative bulk layer (RBL) model to the electrical triple layer (ETL) model, we developed a comprehensive model which could predict the local surface charge density for such simple or complex domain with overlapped or non-overlapped electric double layers. We modeled the streaming conductance in silica nanofluidic channels using the presented numerical framework (PNP + NS). It is shown that for simple straight nanochannel with 140 (nm) height the results would not be significantly changed when the representative bulk layer thickness increased. However, when the height of nanofluidic channel decreased, the proposed framework predicted results that were more accurate for smaller representative bulk layer thickness. We investigated the reverse electro dialysis (RED) phenomenon with inhomogeneous surface charge and overlapped EDLs using the RBL model. The modeling results revealed an interesting phenomenon that the logarithm of the normalized slope of current-voltage (I-V) curve would be roughly increased as a linear function of the ratio of nanochannel length to height. Moreover, it is demonstrated that the logarithm of ion-selective nanochannel current exhibited a linear decreasing relationship with the increasing nanochannel length to height. Inspiring the linear behavior of slope and ion current, we found a dimensionless relation for a current-voltage curve, which was independent of nanochannel length to height variations. Considering the arbitrary selection of representative layer thickness, the RBL model could be utilized to figure out the local electrical boundary condition for simple (nanochannel) or complex (porous media) geometries.

Acknowledgement

This work is financially supported by the NSF grant of China (No. 51676107, 91634107), National Science and Technology Major Project on Oil and Gas (No. 2016ZX05011003).

References

- [1] R.A. Jacobs, M.Z. Sengun, R.E. Hicks, R.F. Probst, Model and experiments on soil remediation by electric-fields, *J. Environ. Sci. Health Part A-Environ. Sci. Eng. Toxic Hazard. Subst. Control* 29 (1994) 1933–1955.
- [2] J.M. Dzenitis, Soil chemistry effects and flow prediction in electroremediation of soil, *Environ. Sci. Technol.* 31 (1997) 1191–1197.
- [3] J.C. Fair, J.F. Osterle, reverse electro dialysis in charged capillary membranes, *J. Chem. Phys.* 54 (1971) 3307–4000.
- [4] P.R. Johnson, N. Sun, M. Elimelech, Colloid transport in geochemically heterogeneous porous media: modeling and measurements, *Environ. Sci. Technol.* 30 (1996) 3284–3293.
- [5] L.M. Vane, G.M. Zang, Effect of aqueous phase properties on clay particle zeta potential and electro-osmotic permeability: implications for electro-kinetic soil remediation processes, *J. Hazard. Mater.* 55 (1997) 1–22.
- [6] D.S. Schultz, Electroosmosis technology for soil remediation: laboratory results, field trial, and economic modeling, *J. Hazard. Mater.* 55 (1997) 81–91.
- [7] A. Revil, P.A. Pezard, P.W.J. Glover, Streaming potential in porous media 1. Theory of the zeta potential, *J. Geophys. Res.-Solid Earth* 104 (1999) 20021–20031.
- [8] A. Revil, H. Schwaeger, L.M. Cathles, P.D. Manhardt, Streaming potential in porous media 2. Theory and application to geothermal systems, *J. Geophys. Res.-Solid Earth* 104 (1999) 20033–20048.
- [9] N. Sun, M. Elimelech, N.Z. Sun, J.N. Ryan, A novel two-dimensional model for colloid transport in physically and geochemically heterogeneous porous media, *J. Contaminant Hydrol.* 49 (2001) 173–199.
- [10] A. Obliger, M. Jardat, D. Coelho, S. Bekri, B. Rotenberg, Pore network model of electrokinetic transport through charged porous media, *Phys. Rev. E* 89 (2014).
- [11] S.J. Kim, S.H. Ko, K.H. Kang, J. Han, Direct seawater desalination by ion concentration polarization, *Nat. Nanotechnol.* 5 (2010) 297–301.
- [12] H. Daiguji, P.D. Yang, A. Majumdar, Ion transport in nanofluidic channels, *Nano Lett.* 4 (2004) 137–142.
- [13] H. Daiguji, P.D. Yang, A.J. Szeri, A. Majumdar, Electrochemomechanical energy conversion in nanofluidic channels, *Nano Lett.* 4 (2004) 2315–2321.
- [14] R. Karnik, C. Duan, K. Castelino, H. Daiguji, A. Majumdar, Rectification of ionic current in a nanofluidic diode, *Nano Lett.* 7 (2007) 547–551.
- [15] C.K. Haluska, K.A. Riske, V. Marchi-Artzner, J.-M. Lehn, R. Lipowsky, R. Dimova, Time scales of membrane fusion revealed by direct imaging of vesicle fusion with high temporal resolution, *PNAS* 103 (2006) 15841–15846.
- [16] R. Dimova, N. Bezlyepkina, M.D. Jordo, R.L. Knorr, K.A. Riske, M. Staykova, P.M. Vlahovska, T. Yamamoto, P. Yang, R. Lipowsky, Vesicles in electric fields: some novel aspects of membrane behavior, *Soft Matter* 5 (2009) 3201–3212.
- [17] D. Lacoste, G.I. Menon, M.Z. Bazant, J.F. Joanny, Electrostatic and electrokinetic contributions to the elastic moduli of a driven membrane, *Euro. Phys. J. E* 28 (2009) 243–264.
- [18] M. Taghipoor, A. Bertsch, P. Renaud, An improved model for predicting electrical conductance in nanochannels, *PCCP* 17 (2015) 4160–4167.
- [19] Y. Ma, L.H. Yeh, C.Y. Lin, L.J. Mei, S.Z. Qian, pH-regulated ionic conductance in a nanochannel with overlapped electric double layers, *Anal. Chem.* 87 (2015) 4508–4514.
- [20] W. Li, N.A.W. Bell, S. Hernandez-Ainsa, V.V. Thacker, A.M. Thackray, R. Bujdoso, U.F. Keyser, Single protein molecule detection by glass nanopores, *ACS Nano* 7 (2013) 4129–4134.
- [21] C.C. Harrell, S.B. Lee, C.R. Martin, Synthetic single-nanopore and nanotube membranes, *Anal. Chem.* 75 (2003) 6861–6867.
- [22] S. Song, A.K. Singh, T.J. Shepodd, B.J. Kirby, Microchip dialysis of proteins using in situ photopatterned nanoporous polymer membranes, *Anal. Chem.* 76 (2004) 2367–2373.
- [23] D. Beamish, R.J. Peart, Electrokinetic geophysics – a review, *Terr. Nova* 10 (1998) 48–55.
- [24] C.Y. Wang, Fundamental models for fuel cell engineering, *Chem. Rev.* 104 (2004) 4727–4765.
- [25] E.V. Dydek, M.Z. Bazant, Nonlinear dynamics of ion concentration polarization in porous media: the leaky membrane model, *Aiche J.* 59 (2013) 3539–3555.
- [26] D.K. Kim, C.H. Duan, Y.F. Chen, A. Majumdar, Power generation from concentration gradient by reverse electro dialysis in ion-selective nanochannels, *Microfluid. Nanofluid.* 9 (2010) 1215–1224.
- [27] Q.S. Pu, J.S. Yun, H. Temkin, S.R. Liu, Ion-enrichment and ion-depletion effect of nanochannel structures, *Nano Lett.* 4 (2004) 1099–1103.
- [28] T.A. Zangle, A. Mani, J.G. Santiago, Theory and experiments of concentration polarization and ion focusing at microchannel and nanochannel interfaces, *Chem. Soc. Rev.* 39 (2010) 1014–1035.
- [29] J.Q. Shang, Zeta potential and electroosmotic permeability of clay soils, *Can. Geotech. J.* 34 (1997) 627–631.
- [30] P.B. Peters, R. van Roij, M.Z. Bazant, P.M. Biesheuvel, Analysis of electrolyte transport through charged nanopores, *Phys. Rev. E* 93 (2016).
- [31] L. Zhang, M. Wang, Electro-osmosis in inhomogeneously charged microporous media by pore-scale modeling, *J. Colloid Interface Sci.* 486 (2017) 219–231.
- [32] M. Wang, S. Chen, Electroosmosis in homogeneously charged micro- and nanoscale random porous media, *J. Colloid Interface Sci.* 314 (2007) 264–273.
- [33] D. Stein, M. Kruihof, C. Dekker, Surface-charge-governed ion transport in nanofluidic channels, *Phys. Rev. Lett.* 93 (2004) 4.
- [34] R. Karnik, K. Castelino, R. Fan, P. Yang, A. Majumdar, Effects of biological reactions and modifications on conductance of nanofluidic channels, *Nano Lett.* 5 (2005) 1638–1642.
- [35] F.H.J. van der Heyden, D. Stein, C. Dekker, Streaming currents in a single nanofluidic channel, *Phys. Rev. Lett.* 95 (2005) 4.
- [36] M. Wang, A. Revil, Electrochemical charge of silica surfaces at high ionic strength in narrow channels, *J. Colloid Interface Sci.* 343 (2010) 381–386.
- [37] A. Kitamura, K. Fujiwara, T. Yamamoto, S. Nishikawa, H. Moriyama, Analysis of adsorption behavior of cations onto quartz surface by electrical double-layer model, *J. Nucl. Sci. Technol.* 36 (1999) 1167–1175.

- [38] W. Stumm, J.J. Morgan, *Aquatic Chemistry: Chemical Equilibria and Rates in Natural Waters*, Wiley, third ed., 1996.
- [39] S.H. Behrens, D.G. Grier, The charge of glass and silica surfaces, *J. Chem. Phys.* 115 (2001) 6716–6721.
- [40] K.-D. Huang, R.-J. Yang, Electrokinetic behavior of overlapped electric double layers in nanofluidic channels, *Nanotechnology* 18 (2007).
- [41] J.A. Davis, R.O. James, J.O. Leckie, Surface ionization and complexation at the oxide/water interface, *J. Colloid Interface Sci.* 63 (1978) 480–499.
- [42] M. Wang, Q. Kang, E. Ben-Naim, Modeling of electrokinetic transport in silica nanofluidic channels, *Anal. Chim. Acta* 664 (2010) 158–164.
- [43] A. Alizadeh, M.E. Warkiani, M. Wang, Manipulating electrokinetic conductance of nanofluidic channel by varying inlet pH of solution, *Microfluid. Nanofluid.* 21 (2017) 52.
- [44] A.J. Brad, L.R. Faulkner, *Electrochemical Methods*, John Wiley & Sons Inc, Hoboken, 2001.
- [45] M. Tasaka, R. Kiyono, A. Taniguchi, Experimental evaluation of single ion activities, *J. Membr. Sci.* 185 (2001) 245–251.
- [46] D.-K. Kim, Numerical study of power generation by reverse electrodialysis in ion-selective nanochannels, *J. Mech. Sci. Technol.* 25 (2011) 5–10.
- [47] A. Alizadeh, L. Zhang, M. Wang, Mixing enhancement of low-Reynolds electroosmotic flows in microchannels with temperature-patterned walls, *J. Colloid Interface Sci.* 431 (2014) 50–63.
- [48] P.C. Lichtner, *Principles and Practice of Reactive Transport Modeling*, Scientific Basis for Nuclear Waste Management XVII, Symposium, 111 (1995) 117–130.
- [49] M. Wang, Q. Kang, Modeling electrokinetic flows in microchannels using coupled lattice Boltzmann methods, *J. Comput. Phys.* 229 (2010) 728–744.
- [50] R. Qiao, N.R. Aluru, Multiscale simulation of electroosmotic transport using embedding techniques, *Int. J. Multiscale Comput. Eng.* 2 (2004) 173–188.
- [51] H. Tian, L. Zhang, M. Wang, Applicability of Donnan equilibrium theory at nanochannel-reservoir interfaces, *J. Colloid Interface Sci.* 452 (2015) 78–88.
- [52] M. Wang, Q. Kang, Electrochemomechanical energy conversion efficiency in silica nanochannels, *Microfluid. Nanofluid.* 9 (2010) 181–190.
- [53] F. Baldessari, J.G. Santiago, Electrokinetics in nanochannels. Part I. Electric double layer overlap and channel-to-well equilibrium (vol 325, pg 526, 2008), *J. Colloid Interface Sci.* 331 (2009). 549–549.
- [54] R.B. Schoch, P. Renaud, Ion transport through nanoslits dominated by the effective surface charge, *Appl. Phys. Lett.* 86 (2005) 253111.